

# **Representation of the Broad-Scale Spectral Form in the Two-Scale Approximation for the Full Boltzmann Integral**

**Charles E. Long, US Army ERDC-CHL, Duck, NC (US)**  
**Donald T. Resio, US Army ERDC-CHL, Vicksburg, MS (US)**

## **1. Introduction**

As described in Resio and Perrie (2008) and Perrie and Resio (2009), the Two-Scale Approximation (TSA) to the Full Boltzmann Integral (FBI) solution (Hasselmann, 1962; Zakharov and Filenenko, 1966) for wave-wave interactions in wind-driven seas decomposes directional spectra into two parts, a broad-scale form (parametric - with a limited number of degrees of freedom) and a superposed local-scale (non-parametric - which retains all of the degrees of freedom in a modeled directional spectrum). Such an approximation utilizes a discrete set of parameter values in the approximation for the broad-scale portion of the spectrum. This, in turn, raises the question of how many parameters and how many discrete values of these parameters are needed to provide an accurate approximation for operational purposes? To answer this question, one must first examine the inherent variability in natural spectra within a single, wind-sea spectrum and then examine the potential interaction between co-existing wave trains. Then, the ability of the second scale within the TSA must be understood in order to understand what the impacts of unresolved spectral energy within the first scale on the total estimate.

In this paper, we will begin with a brief description of the TSA and some of storage requirements for pre-calculated information. We will then examine the number of parameters (dimensions) required for a robust parameterization of directional spectra based on analyses of various sets of directional spectra from around the world. Next, some results from a numerical study of interacting wave trains will be described, along with typical coastal spectra. Finally, all of this will be discussed within the context of a new operational source term for operational wave modeling.

## **2. The TSA and computer storage requirements**

Given the two-component decomposition used by Resio and Perrie (2008), it can be shown that by interaction integral can be subdivided into two parts, one part which contains the interactions due to the broad-scale (parameterized) portion of the spectrum and a second part which contains the interactions due to the small-scale (perturbation) portion of the spectrum and the “cross-interactions” between the broach scale energies and the perturbation energies. Equation 1 shows the basic form of this subdivision

$$\frac{\partial n_1}{\partial t} = B + \left(\frac{k}{k_0}\right)^{19/2} \left\langle \left(\frac{\beta}{\beta_0}\right) \iint (\hat{n}_1 n'_3 + n'_1 \hat{n}_3 + n'_1 n'_3) \Lambda_p(\hat{n}_2 - \hat{n}_4, \underline{k}_1, k_*, \theta_*, x_1, \dots, x_n) k_* d\theta_* dk_* \right. \\ \left. + \left(\frac{\beta}{\beta_0}\right)^2 \iint (n'_1 - n'_3) \Lambda_d(\hat{n}_2 \hat{n}_4, \underline{k}_1, k_*, \theta_*, x_1, \dots, x_n) k_* d\theta_* dk_* \right\rangle$$

where

$$\Lambda_p(\hat{n}_2 - \hat{n}_4, \underline{k}_1, k_*, \theta_*, x_1, \dots, x_n) = \iint C \left| \frac{\partial W}{\partial n} \right|^{-1} (\hat{n}_4 - \hat{n}_2) ds$$

$$\Lambda_d(\hat{n}_2 \hat{n}_4, \underline{k}_1, k_*, \theta_*, x_1, \dots, x_n) = \iint C \left| \frac{\partial W}{\partial n} \right|^{-1} \hat{n}_2 \hat{n}_4 ds$$
(1)

and where  $\left(\frac{\beta}{\beta_0}\right)$  is the ratio of the actual steepness to a reference steepness for the large-

scale spectral component and  $\theta_*$  and  $k_*$  are defined as

$$\theta_* = \theta_3 - \theta_1$$

and

$$k_* = \left(\frac{k_3 - k_1}{k_p}\right)$$

The first term on the right-hand side of equation 1 contains the interactions for the parameterized spectrum while the second term on the right-hand side contains the remaining interactions. Three terms in equation 1,  $B$ ,  $\Lambda_p$ , and  $\Lambda_d$  all have to be pre-computed if this algorithm is to be efficient. In tests conducted to date, a typical storage requirement for a single pre-calculated case for all three matrices in straightforward binary form is in the range of 0.5 to 1.5 megabytes depending on details of the integration limits. This could be reduced somewhat by the use of non-standard storage methods; however, given the size of computer memories, this may not be necessary.

### 3. Characteristics of Spectra in Nature

Parametric forms for directionally integrated wave spectra have evolved considerably since wave spectra began to be measured in the 1940's and 1950's. In deep water, for dimensional consistency, the spectrum is typically written in terms of a power law in frequency with appropriate coefficients. The JONSWAP spectrum (Hasselmann, 1972) is an extension of the Pierson-Moskowitz spectral form (Pierson and Moskowitz, 1964) and can be written in terms of an  $f^{-5}$  power law,

$$E(f) = \frac{\alpha g^2}{(2\pi)^4} f^{-5} \exp \left[ -1.25 \left( \frac{f}{f_p} \right)^4 \right] \gamma_5^{\Theta_5}$$

where  $E(f)$  is the spectral energy density at  $f$ ,

$$\Theta_5 = \exp \left[ \frac{-(f - f_p)^2}{2\sigma^2 f_p^2} \right] \quad (2)$$

and

$$\begin{aligned} \sigma &= \sigma_a \text{ for } f < f_p \\ &= \sigma_b \text{ for } f \leq f_p \end{aligned}$$

In equation 2,  $\alpha$  is a dimensionless constant and the typical values of  $\sigma_a$  and  $\sigma_b$  are taken to be 0.07 and 0.09, respectively. Most recent studies, however, have found that wave spectra follow an  $f^{-4}$  power law (Toba, 1978; Donelan *et al.*, 1985; Resio and Perrie, 1989; Resio *et al.* 2004; Long and Resio, 2007). A simplified version of the Resio-Perrie spectral form (Figure 1) can be written as

$$E(f) = \frac{2\beta g}{(2\pi)^3} f^{-4} \left[ z_4 \left( \frac{f}{f_p} \right)^4 \exp(-\Theta_4) + 1 \right]^{3/2}$$

where

$\beta$  is the equilibrium range constant as defined in Resio *et al.* (2004)

$z_4$  is a constant  $= \gamma_r$  for  $f \leq f_p$ ;  $\gamma_r - 1$  for  $f > f_p$

$\gamma_r$  is the relative peakedness as defined in Long and Resio (2007)

$\Theta_4$  is a peakedness factor given by

$$\Theta_4 = \left[ \frac{(f - f_p)^2}{2\sigma f_p} \right]^2$$

with values the same as for the JONSWAP spectrum.

Resio and Long (2007) presented evidence that there was a transition from an  $f^{-4}$  form to an  $f^{-5}$  form at high frequencies, particularly for the case of highly peaked spectra. Additionally, analyses performed by Long and Resio (2007) showed that many aspects of directionally integrated spectral shape could all be linked directly to spectral peakedness, which in turn was closely coupled to the inverse wave age  $u/c_p$  where  $u$  is windspeed and  $c_p$  is the phase speed of the spectral peak (Figure 2). In light of these results and given that both peak frequency and the equilibrium range coefficient can be continuously scaled into the TSA results, and therefore do not have to be parameterized, spectral peakedness was selected as the primary parametric factor that needed to be incorporated into the TSA broad-scale, pre-calculated functions.

In terms of directional distributions, Long and Resio also found that the angular separation was a function of peakedness and preliminary findings suggested that the degree of bimodality is also a strong function of spectral peakedness, with the bimodality being very pronounced in spectra with high peakedness and low as the relative peakedness,  $\gamma_r$ , approached a fully-developed value of approximately 1. Additional analyses performed for this paper have shown that the “gross-scale” characteristics of the directional spectrum measure in the Long and Resio study are actually quite consistent with the directional distribution hypothesized by Hasselmann *et al.* (1980). Figure 3 shows a comparison of the values of “ $n$ ” as a function of  $\frac{f}{f_p}$  using a  $\cos^{2n}$  basis for the Currituck Sound bimodal spectra to the Hasselmann *et al.* (1980) results. As can be seen here, the bimodal spectrum, when analyzed with a  $\cos^{2n}$  basis shows that the gross characteristics of the bimodal spectrum (associated with short-fetch/duration, high-peakedness situations) is relatively similar to the gross characteristics of the spectra typically presumed to be non-bimodal (associated with long fetch/duration, low-peakedness situations).

Based on the results of our analyses, it appears that a single parameter, peakedness, can probably capture most of the “broad-scale” attributes of directional wave spectra in single-peaked local seas, when combined with appropriate scales for the equilibrium range coefficient and spectral peak frequency. As shown in Resio and Perrie (2008) and Perrie and Resio (2009), the second scale of the TSA does a fairly good job of compensating for deviations between the actual spectrum and the broad. For example, Figure 4 shows the case of using a unimodal directional distribution in place of the measured, very-bimodal spectrum in one of the test cases. In the critical spectral peak region, the estimate of  $S_{nl}$  using the parametric term alone deviates from the Full Boltzmann Integral (FBI) by a factor of over 3; however, almost all of this deviation is compensated for by the inclusion of the second term in the TSA. Similarly, in Figure 5, also from Perrie and Resio (2009), the measured spectrum contains a significant shift in its directional characteristics as a function of frequency; yet the combined 2 terms reduce the overall error to less than 5% in the spectral peak region.

It is well known that wave spectra change their shapes as they propagate from deep to shallow water. Consequently, although the a first approximation for the broad-

scale component of  $S_{nl}$  in deep water might be based on peakedness alone, in conjunction with peak frequency and the equilibrium range coefficient, it is necessary to consider an appropriate scaling for depth effects in order to make this approximation to  $S_{nl}$  effective in coastal areas. Consequently, in addition to discrete peakedness variations considered in all the pre-computed terms, it will be necessary to use a suitable scaling parameter, such as  $k_p h$ , to account for depth effects. Numerical studies suggest that about 10-15 discrete values over the range from  $k_p h = 0.45$  to  $k_p h = 2.5$  provides an accuracy within 15% or so for  $S_{nl}$ . Onorato *et al.* (2008) showed that 4-wave interactions still play the dominant role in shallow water for the case of resonant interactions, so the proper treatment of this term in shallow water is likely to be critical to nearshore wave predictions.

As noted in the original derivation by Herterich and Hasselmann (1980) and subsequently discussed in Resio and Perrie (2008), the current method used to scale the DIA is not suitable for  $k_p h > 1$ , where  $k_p$  is the wavenumber associated with the spectral peak and  $h$  is water depth. For a wave spectrum with a peak wave period of 10 seconds, the DIA's depth scaling becomes extremely inaccurate in depths less than about 20 meters; and for a peak wave period of 13 second the limit to the applicability is about 32 meters. Since, this term is presently used in all of the primary Third-Generation wave models today, it is reasonable to hypothesize that the effects of nonlinear interactions in coastal waters are simple not included within these models and other source terms must be tuned to compensate for this absence.

To provide some perspective on characteristic variations in single peaked spectra in shallow water, we examined a large set of single peaked spectra from the waverider in a depth of about 17 meters, about 5 km offshore from the Field Research Facility in Duck, North Carolina. Since these data are in intermediate depths, it is important to use wavenumber scaling rather than frequency scaling. Two sets of typical spectra scaled according to a compensated wavenumber form ( $F_c(k) = F(k)k^{5/2}$ , where  $F_c$  is the compensated wave spectrum,  $F$  is the wavenumber spectrum, and  $k$  is wavenumber) are shown in Figures 6 and 7. As can be seen here, the low-peakedness spectra and high-peakedness spectra both contain  $k^{-5/2}$  equilibrium ranges; however, similar to what has been observed in deep-water high, the high-peakedness case appears to transition to a  $k^{-3}$  ( $f^{-5}$ ) form at high frequencies.

#### 4. Mixed sea and swell in coastal areas

Up to this point we have focused on directionally integrated spectra that contain only a single peak. In this section we will examine the relative role of the cross interactions between a wind sea and a coexistent swell. For simplicity, we will focus on sea and swell cases that are aligned in the same direction, since this represents the potential for maximum effects on the nonlinear interactions. Three different swell spectra, with peak frequencies of 0.051 Hz, 0.67 Hz, and 0.76 Hz, are superposed in turn over a sea spectrum with a peak frequency of 0.1 Hz as shown in Figure 8. In each case,

the peak energy set to the same value. Figure 9 shows the calculated values of  $S_{nl}$  for the three test cases. Clearly, the swell spectrum with the 0.051 Hz spectral peak has essentially zero effect on waves in the vicinity of the local sea peak and the swell spectrum with a peak of 0.67 Hz has only a very slight effect. However, the effects of the swell with a 0.76 Hz spectral peak are significant.

A second numerical experiment was conducted with the equilibrium range coefficient in the swell set to a proportion of the equilibrium range coefficient in the sea while maintaining a peak spectral frequency of 0.04 Hz (Figure 10). In this case, the separation of the two peaks precludes strong interactions between the peaks and it only the effect of the superposed equilibrium ranges is considered. The full integral solution (Figure 11) shows that the effects are relatively minor for this case.

## **5. Directionally aligned, mixed sea and swell spectra at Duck**

As a final “sanity check” on some of the ideas examined here, we selected a sequence of spectra from the waverider in which the spectral peak regions were aligned. Figures 12 - 18 show the directionally integrated spectra for at somewhat irregularly spaced intervals (selected to capture the primary variations that occurred) for this case. As can be seen here, the spectra appear to be quite irregular and reasonable typical of situations with two dominant wave trains coexistent. In these plots, all the spectra are scaled to the same maximum value to provide a consistent perspective on what is taking place. The lighter of the two vertical dashed lines on these plots represents the location of the “local sea” spectral peak, while the darker line represents the estimated full-developed limiting frequency for the observed wind speed (with a default lowest value of 0.0425). For reference, the total wave height, wind speed, and estimated limiting wind sea peak frequency ( $f_{10}$ ) are also shown on these plots (with the same default lowest value).

This sequence begins At 0100 on October 14<sup>th</sup> in 2002 where we see two separate spectral peak regions, one around 11 seconds (presumably swell from some relatively close storm) and a second peak around 5.5 seconds. At this time, the two wave trains contain about equal energy. Six hours later at 0700 on the same day, the sea peak has grown considerably over the previous value shown; but twelve hours later the wind speeds have dropped substantially and the sea peak has decayed to a level that is lower than the swell peak. Fifteen hours later (1000 on the 15<sup>th</sup>), the sea and swell separation has become quite pronounced. At this time the wind speeds are increasing and three hours later (1300 on the 13<sup>th</sup>) the sea peak has once again become dominant. As the wind speed continues to rise from about 13 m/sec up to 17 m/sec over the next nine hours, the peakedness of the sea peak continues to increase and the peak energy of the sea becomes substantially higher than the swell peak. In fact, by 2200, the local sea portion of the spectrum has almost overrun the swell spectrum.

To examine these spectra in the context of self-similar pattern of the type associated with wave-wave interactions (Resio *et al.*, 2001; Badulin *et al.*, xxxx), compensated spectra over the same sequence are plotted in the upper panel of Figures 19 – 25 and the mean direction as a function of frequency is plotted in the lower panels. To give some perspective on the effects of refraction on wave directions, the zero reference in the lower panels is taken as shore normal. In the upper panel, a horizontal line has been added which gives the estimated value for the equilibrium range coefficient based on the formulation by Resio *et al.* (2004). In the lower panel, a horizontal line representing the wind direction has been added.

Three aspects of these plots are immediately obvious. First, as expected, compensated energies within the swell portion of these waves are much lower than those in the local seas. Second, although the directions eventually align quite nicely in this sequence, this sequence also contains intervals in which the directions of the two wave trains deviate significantly. Third, the form of the local sea spectrum follows the  $k^{-5/2}$  similarity law very nicely, even for the complex case with significant superposed swell. In fact, even the peakedness characteristics remain quite similar with the high peakedness cases (1900 and 2200 on the 15<sup>th</sup>) producing the same type of short equilibrium ranges transitioning into  $k^{-3}$  high-frequency tails.

## 6. Discussion

There are at least two very different paths that the development of an operational version of the TSA could take. First, one could just come up with a set of  $n$  parameters covering every type of variation observed to occur in natural spectra and use this set as a basis to create the pre-calculated broad-scale matrices required by this method. Second, the method that is followed here, one could determine the primary self-similar spectral forms observed in nature and allow the second scale in the TSA to nudge the spectrum in the appropriate direction. To accomplish this, it is important for the relaxation from a perturbation to follow approximately the same form as the full integral solution. Figures 26 and 27 show that this is indeed the case for the TSA.

From the numerical study of mixed sea and swell, it seems that it might be helpful include a simple parametric representation for spectra when the ratio of the swell peak frequency to the sea peak frequency is larger than about 0.7. Ongoing numerical studies are currently investigating the ability of the second scale within the TSA to handle such perturbations without the need for this additional parametric term, but these have not been completed to date.

## 7. Conclusions

It is clear the TSA has not been optimized for operational applications. At the same time, many comparisons have shown that even in its existing form it consistently outperforms the current method for estimating  $S_{nl}$  in existing operational models,

particularly in shallow water. Some very preliminary findings in this study suggest the following:

1. The form of wind-wave spectra, even in mixed sea-swell situations in near-coast areas, seems to be reasonably captured and very consistent with the similarity forms for spectra in finite depth; however, it is likely that this may not be the case in very steep-sloping coastal areas and perhaps not for very narrow swell peaks that are undergoing strong shoaling.
1. Two parameters (peakedness and relative depth) are probably sufficient to provide adequate estimates of  $S_{nl}$  for general operational purposes (perhaps to depths of 5 meters or so). The total storage estimated for relatively high resolution pre-calculated matrices (for example: 35 frequencies and 36 angles) is only about 250 gigabytes, which certainly presents no problems to modern computers.
2. The ability of a TSA formulation based on self-similar spectral forms seems to offer significant advantages over a method based on arbitrary spectral forms, since the growth in simple situations has been shown to be well-governed by the self-similarity laws.

## REFERENCES

- Donelan, M. A., J. Hamilton and W. H. Hui, 1985: Directional spectra of wind-generated waves, *Phil. Trans. R. Soc. Lond., A*, **315**, 509-562.
- Hasselmann, D.E., Dunkel, M. and J.A. Ewing, 1980: Directional wave spectra observed during JONSWAP 1973, *J. Phys. Oceanogr.* **11**, 718-728.
- Hasselmann, K., 1962: On the nonlinear energy transfer in a gravity wave spectrum, Part 1, *J. Fluid Mech.*, **12**, 481–500.
- Hasselmann, K., Barnett, T.P., Bouws, E., Carlson, H., Cartwright, D. E., Enke, K., Ewing, J. A., Gienapp, H., Hasselmann, D. E., Kruseman, P., Meerburg, A., Muller, P., Olbers, D. J., Richter, K., Sell W., and Walden, H., 1973: Measurements of wind-wave growth and swell decay during the Joint North Sea Wave Project (JONSWAP), *Ergänzungsheft zur Deutschen Hydrographischen Zeits.*, **12**, Reihe A8, 95 pp., 1973.
- Hasselmann, S., Hasselmann, K. Allender, J. H., and Barnett, T. P., 1985: Computations and parametrizations of the nonlinear energy transfer in a gravity-wave spectrum, Part II, Parameterizations of the nonlinear energy transfer for application in wave models, *J. Phys. Oceanogr.*, **15**, 1378–1391.
- Herterich, K., and K. Hasselmann, 1980: A similarity relation for the nonlinear energy transfer in a finite-depth gravity-wave spectrum, *J. Fluid Mech.*, **97**, 215-224.
- Long, C.E. and D.T. Resio, 2007: Wind wave spectral observations in Currituck Sound, North Carolina. *J. Geophys. Res.*, **112**, doi:1029/2006JC003835.
- Onorato, M., Osborne, A. R., Janssen, P. A. E. M. & Resio, D.: 2009, Four-wave resonant interactions in the classical quadratic Boussinesq equations, *J. Fluid Mech.*, **618**, 263-277.
- Perrie, W. and D.T. Resio, 2009: A two-scale approximation for nonlinear energy fluxes in a wind wave spectrum Part II , accepted for publication in *J. Phys. Oceanogr.*
- Pierson, W.J. and L. Moskowitz, 1964: A proposed spectral form for fully developed wind seas based on the similarity theory of S.A. Kitaigorodskii, *J. Geophys. Res.* **69**, 5181-5190.
- Resio, D. T. and W. Perrie, 1989: Implications of an  $f^{-4}$  equilibrium range for wind-generated waves, *J. Phys. Oceanogr.*, **19**, 193-204.
- Resio, D. T. and W. Perrie, 1991: A numerical study of nonlinear energy fluxes due to wave-wave interactions. Part 1. Methodology and basic results, *J. Fluid Mech.*, **223**, 609-629.
- Resio, D. T., J. H. Pihl, B. A. Tracy and C. L. Vincent, 2001: Nonlinear energy fluxes and the finite depth equilibrium range in wave spectra, *J. Geophys. Res.*, **106**, 6985-7000.
- Resio, D.T. and W. Perrie, A two-scale approximation for nonlinear energy fluxes in a wind wave spectrum Part I , *J. Phys. Oceanogr.* 2008., Volume 38 (11), 2801-2816.
- Toba, Y, 1978: Stochastic form of the growth of wind waves in a single-parameter representation with physical implications, *J. Phys. Oceanogr.*, **8**, 494-507.
- Zakharov, V. E. and N. N. Filonenko, 1966: The energy spectrum for stochastic oscillation of a fluid's surface, *Dokl. Akad. Nauk.*, **170**, 1992-1995.

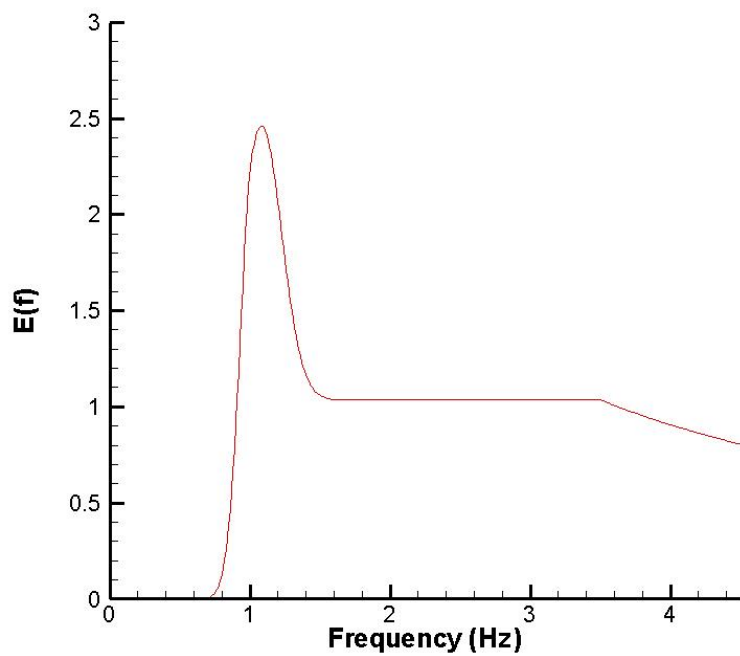


Figure 1. Idealized  $f^{-4}$  form for spectrum.

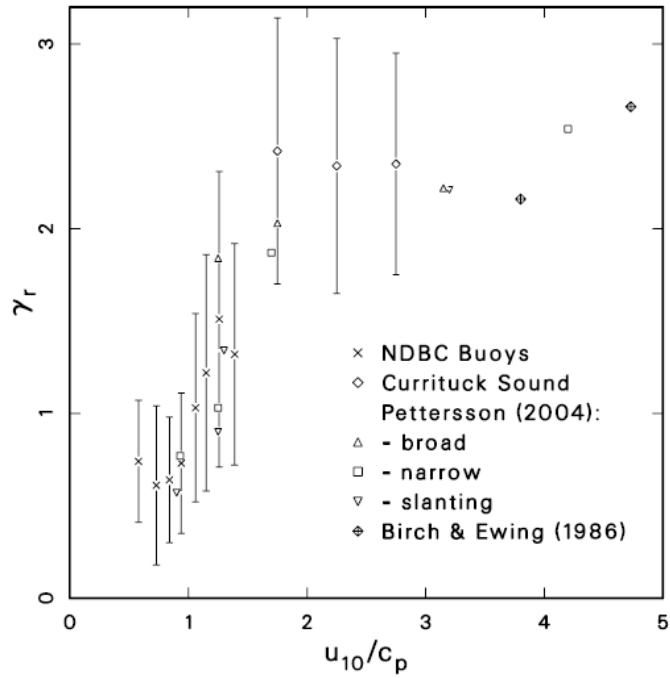


Figure 2. Observed relationship between spectral peakedness and inverse wave age (Long and Resio, 2007)

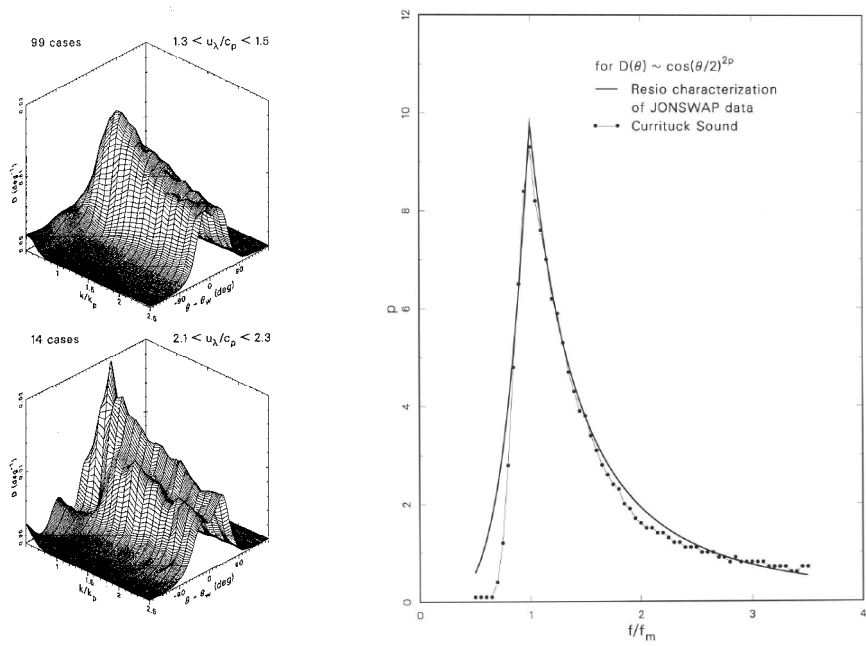


Figure 3. Top left panel shows directional distribution of spectra with low inverse wave age (old waves) from Long and Resio (2007). Bottom left panel shows directional distribution of spectra with high inverse wave age (young waves). The right hand panel shows the variation in “n” obtained when fitting the bottom left hand panel with a  $\cos^{2n}$  function compared to the data from Hasselmann *et al* (1980).

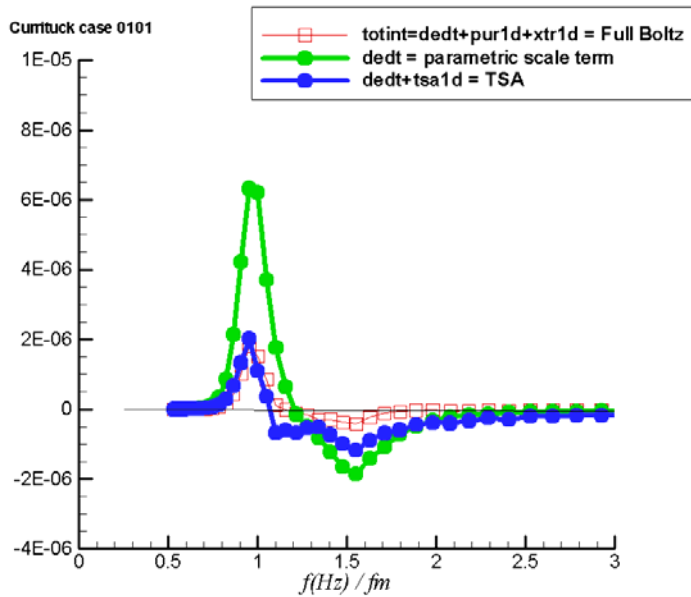


Figure 4. Comparison of parametric term alone in TSA (green line) versus parametric plus second term in the TSA (blue line) to the full integral solution (red line).

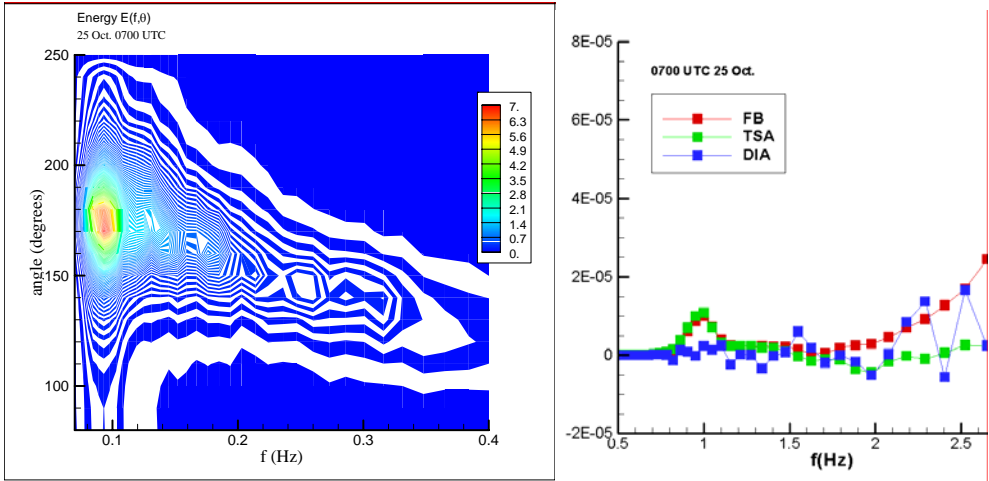


Figure 5. Right hand panel shows a spectrum with strong directional shear and the left hand panel shows the resulting TSA estimate (green) for this spectrum compared to the FBI (red) and the DIA (blue).

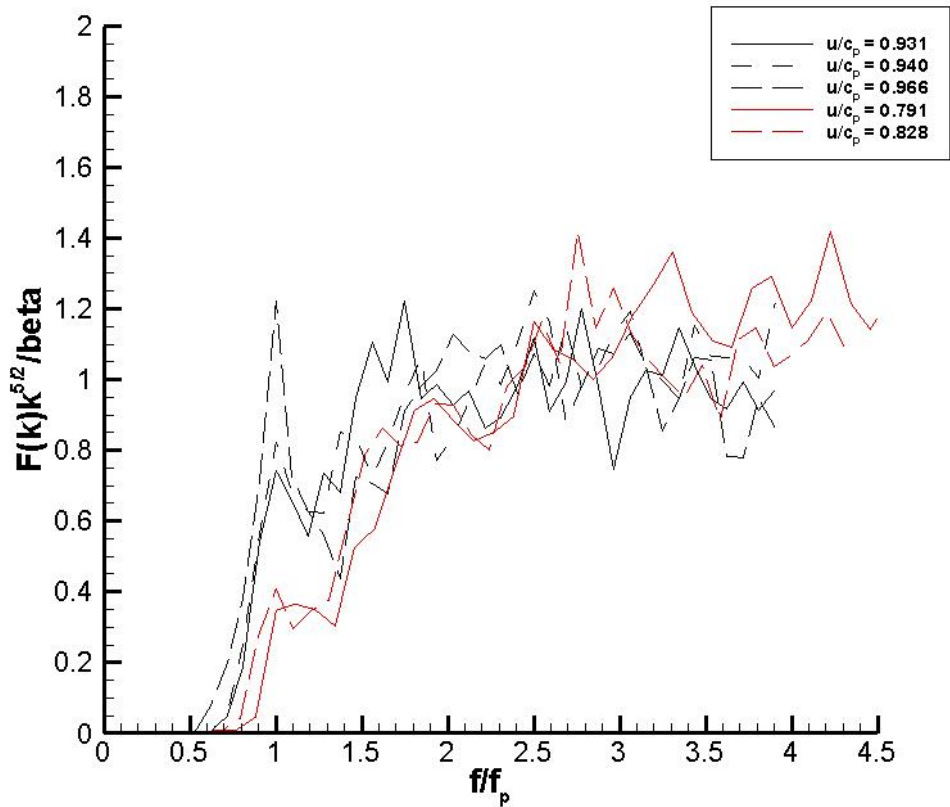


Figure 6. Compensated low-peakedness spectra from waverider in 17 meter depth off of Duck, NC.

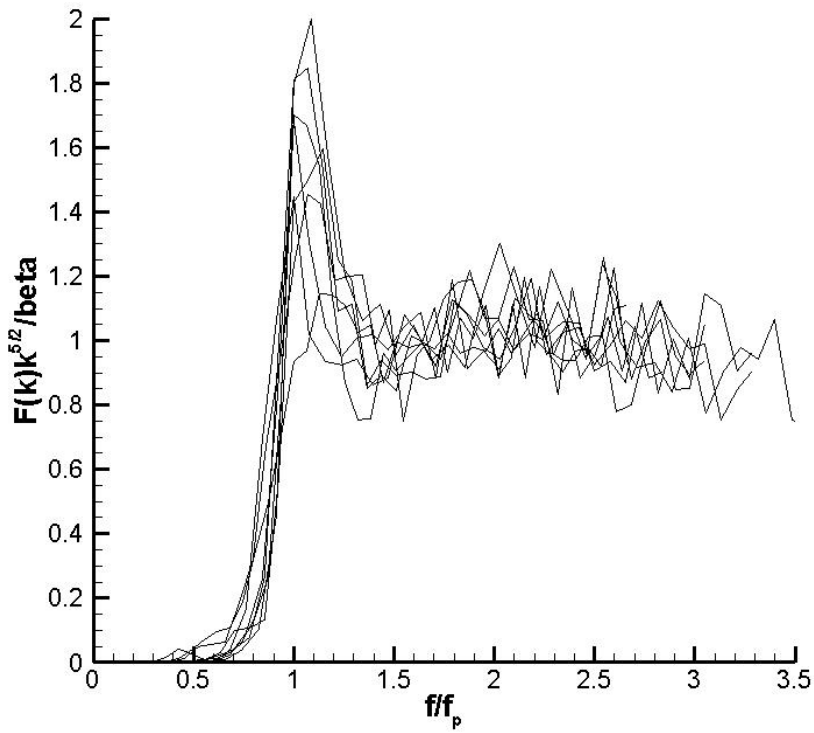


Figure 7. Compensated high-peakedness spectra from waverider in 17 meter depth off of Duck, NC.

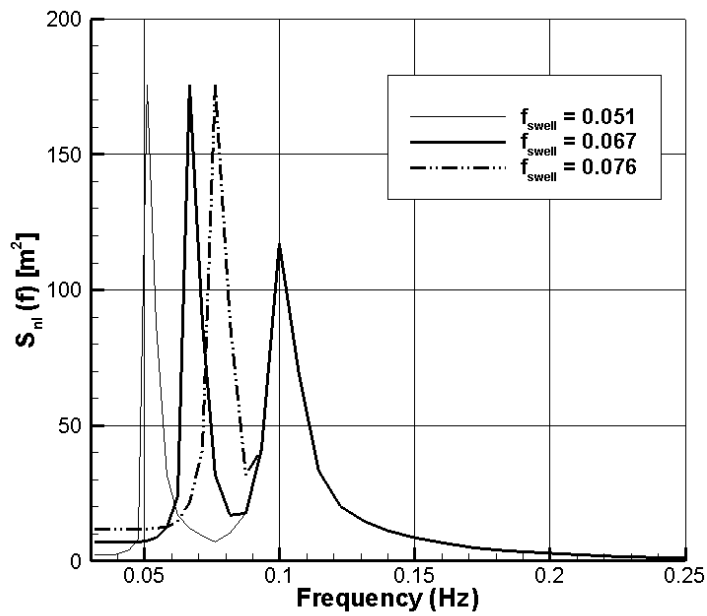


Figure 8. Three spectra used in numerical experiment to test the effects of superposed swell on total nonlinear interactions.

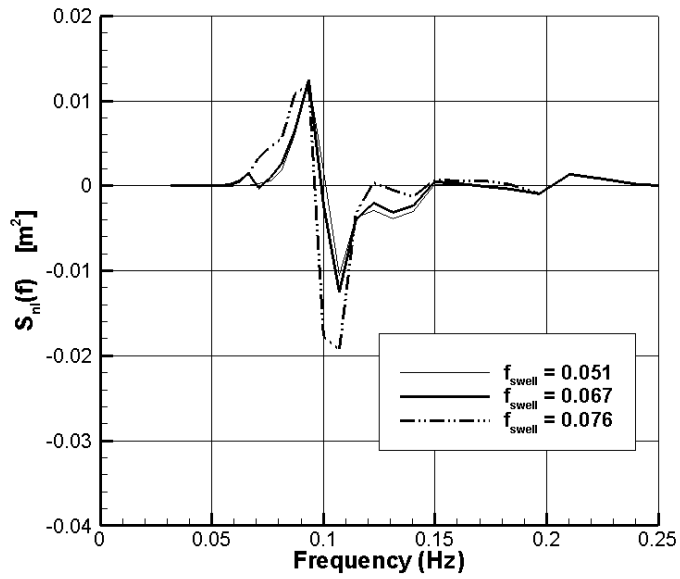


Figure 9. Total nonlinear interactions for the three spectra shown in Figure 8.

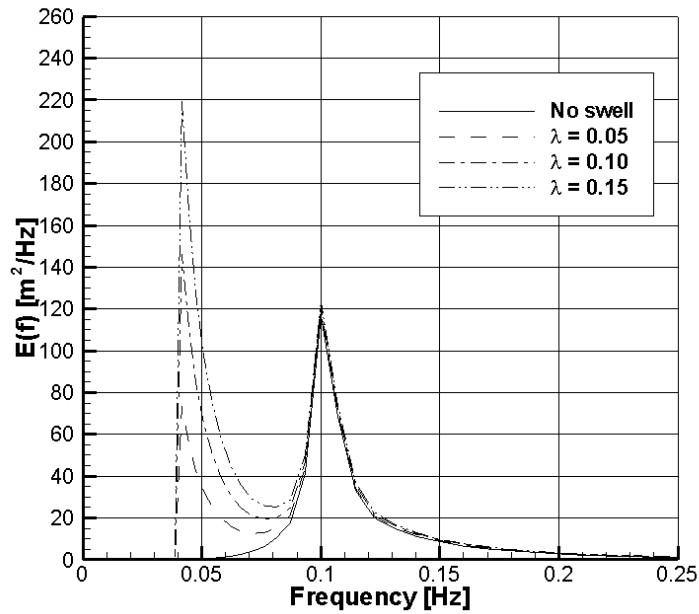


Figure 10. Wave spectra used to test the effects of different swell steepnesses on total nonlinear interactions.

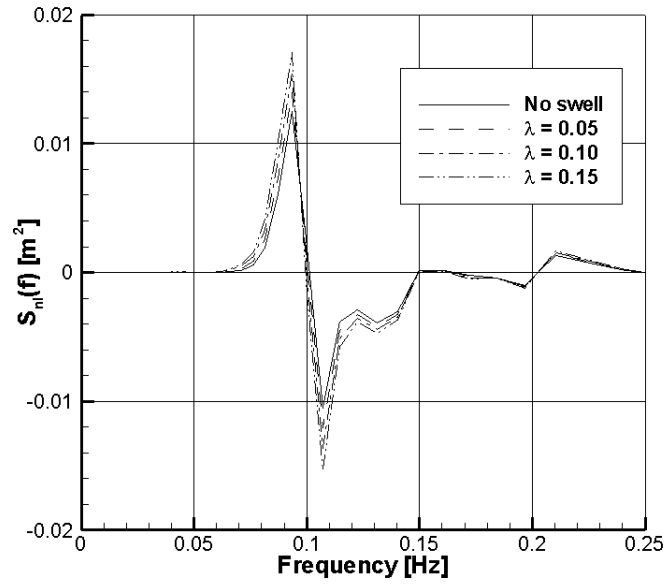


Figure 11. Total nonlinear interactions for the three different swell steepnesses shown in Figure 10.

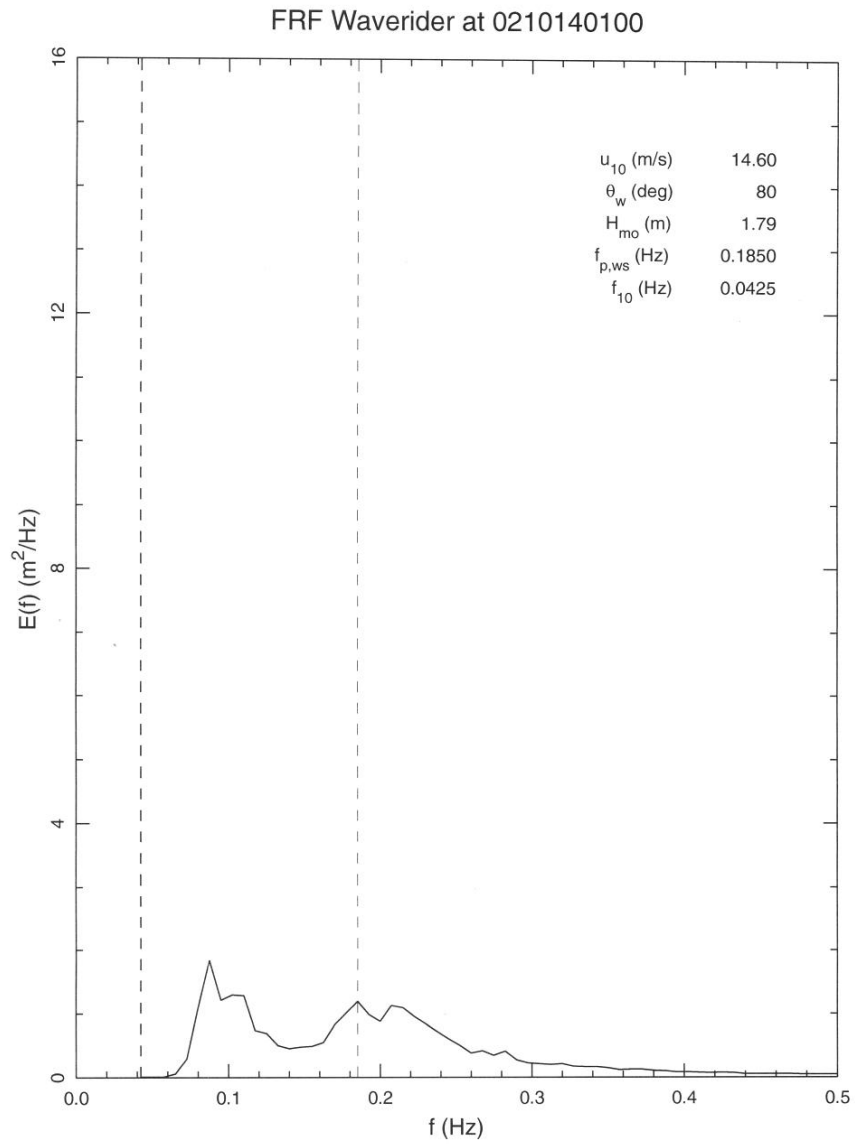


Figure 12. Waverider spectrum at 0100 October 14, 2002.

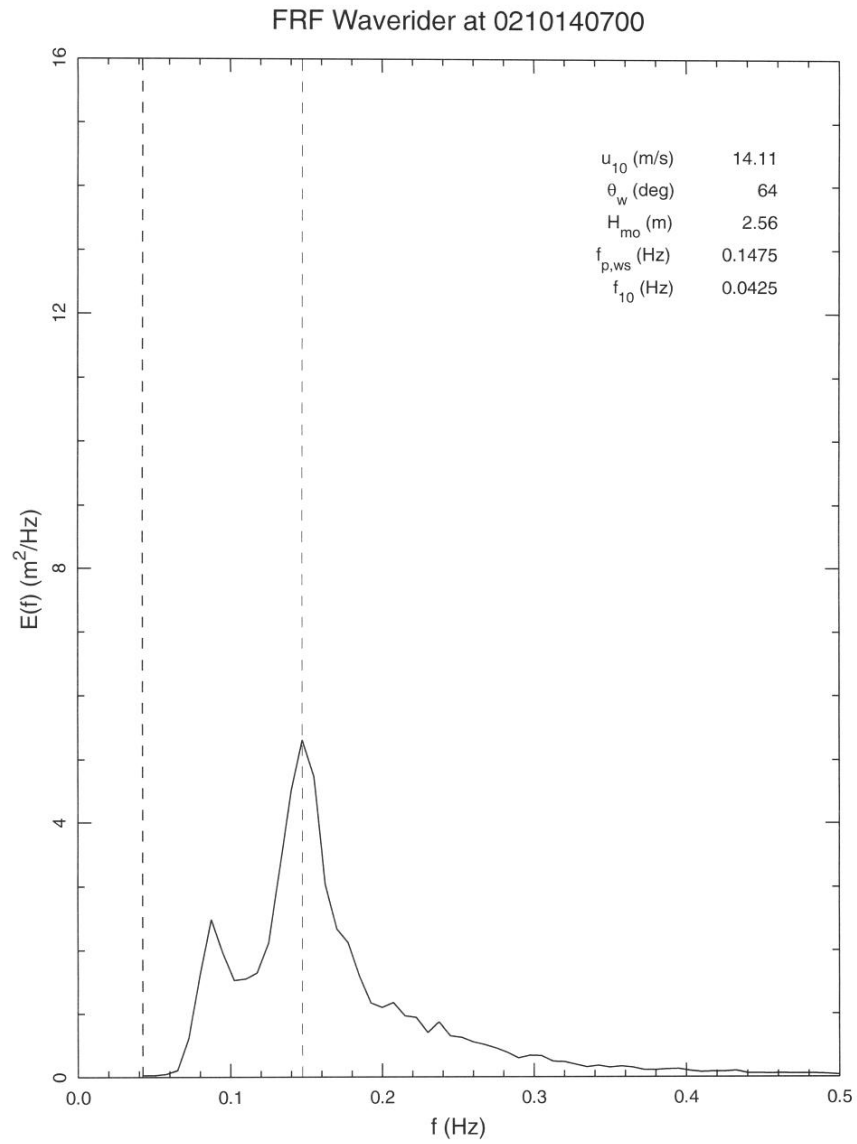


Figure 13. Waverider spectrum at 0700 October 14, 2002.

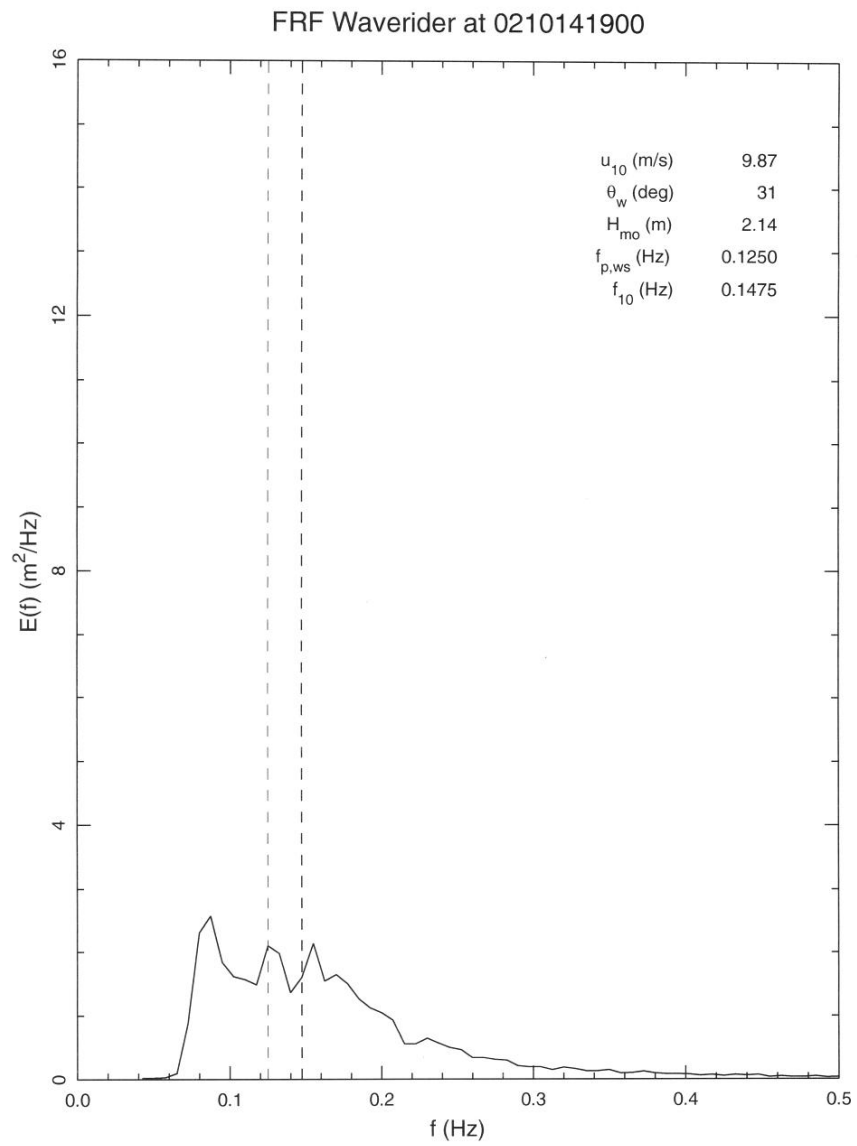


Figure 14. Waverider spectrum at 1900 October 14, 2002.

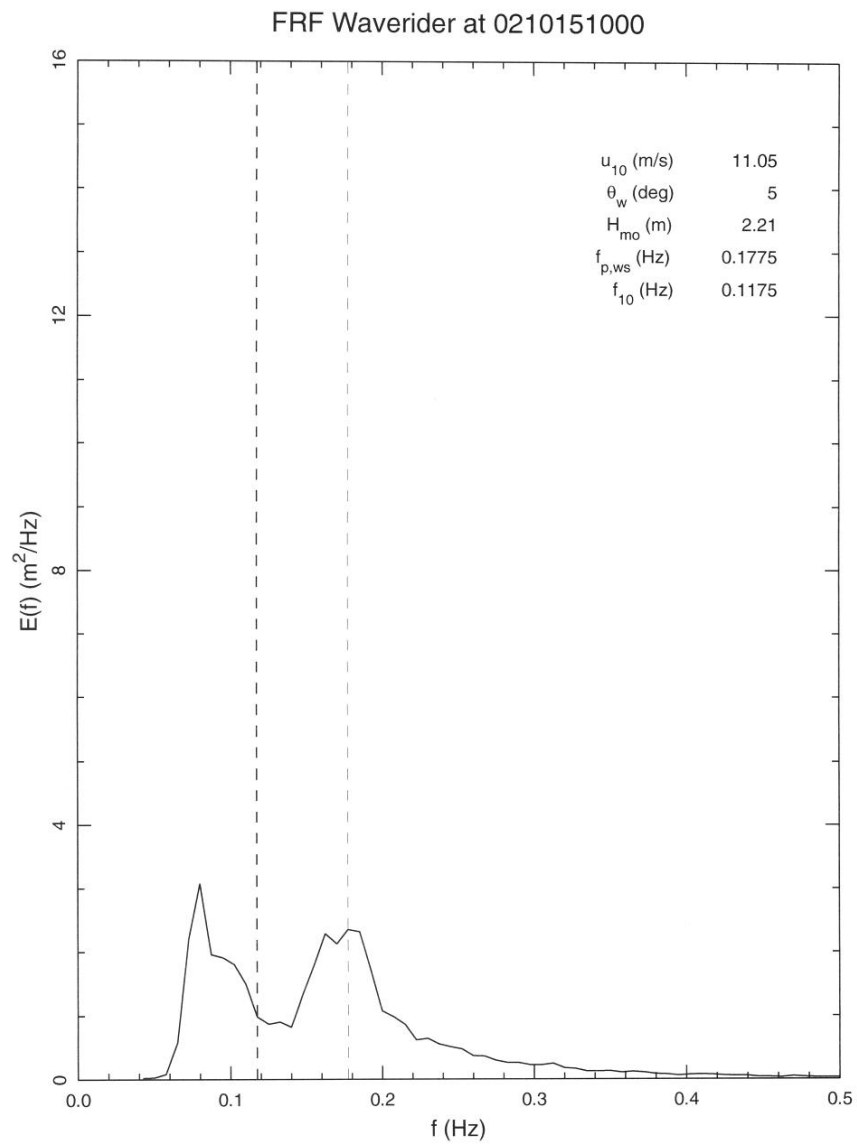


Figure 15. Waverider spectrum at 1000 October 15, 2002.

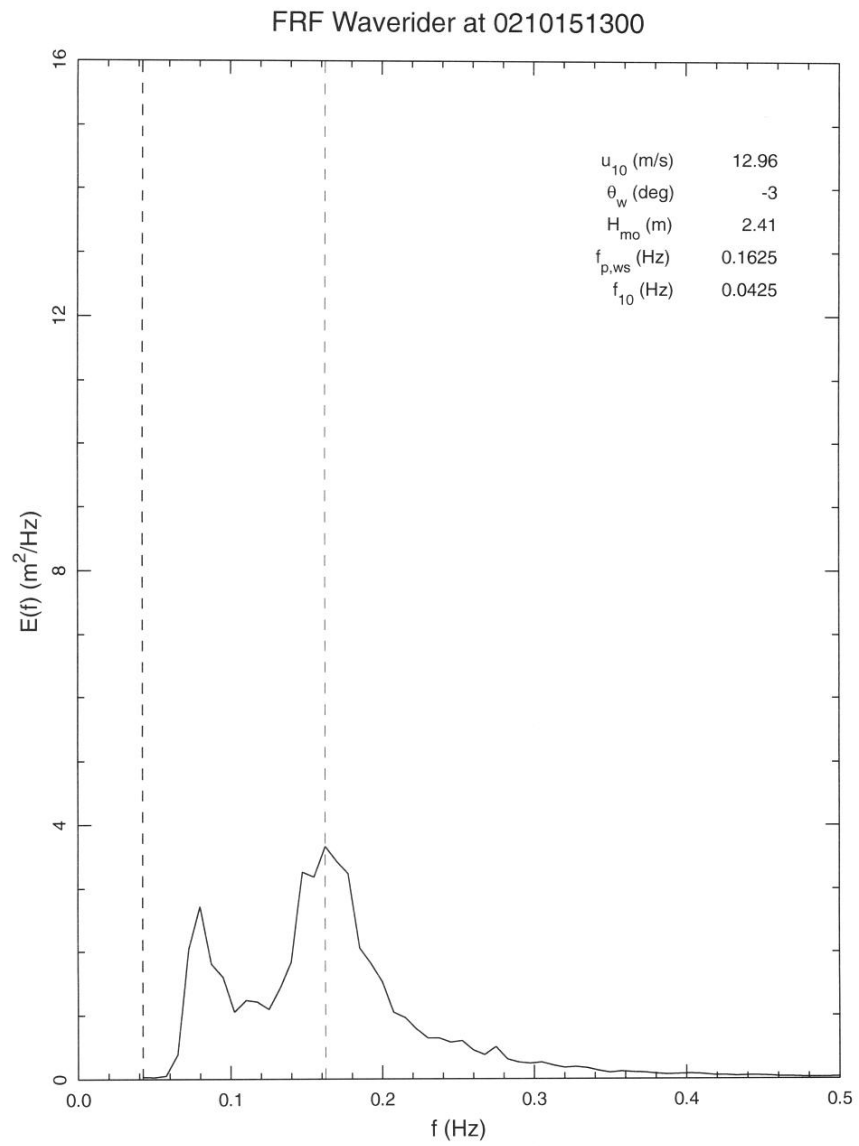


Figure 16. Waverider spectrum at 1300 October 15, 2002.

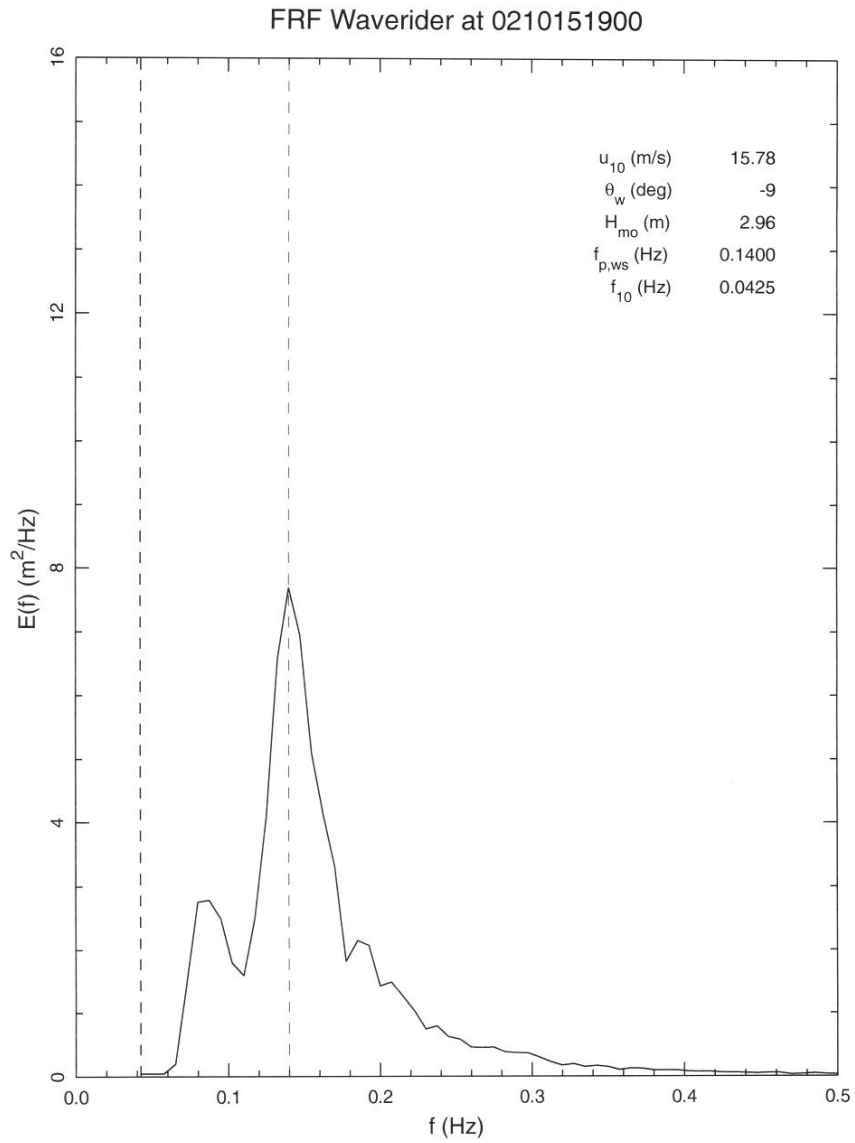


Figure 17. Waverider spectrum at 1900 October 15, 2002.

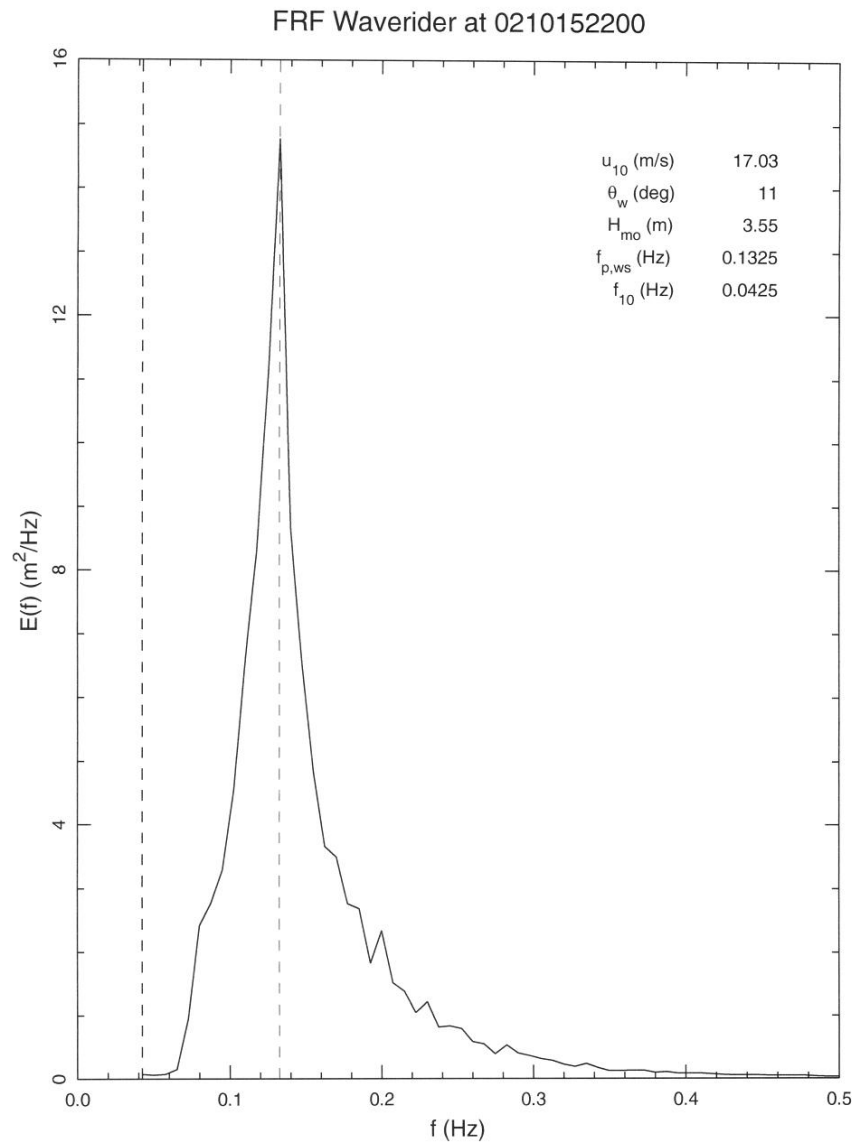


Figure 18. Waverider spectrum at 2200 October 15, 2002.

FRF Waverider at 0210140100

	$H_{mo}$ (m)	$f_{p,ws}$ (Hz)	$\theta_p$ (deg)	$u_{10}$ (m/s)	$\theta_w$ (deg)	$h$ (m)
WR	1.79	0.1850	17	14.60	80	17.0

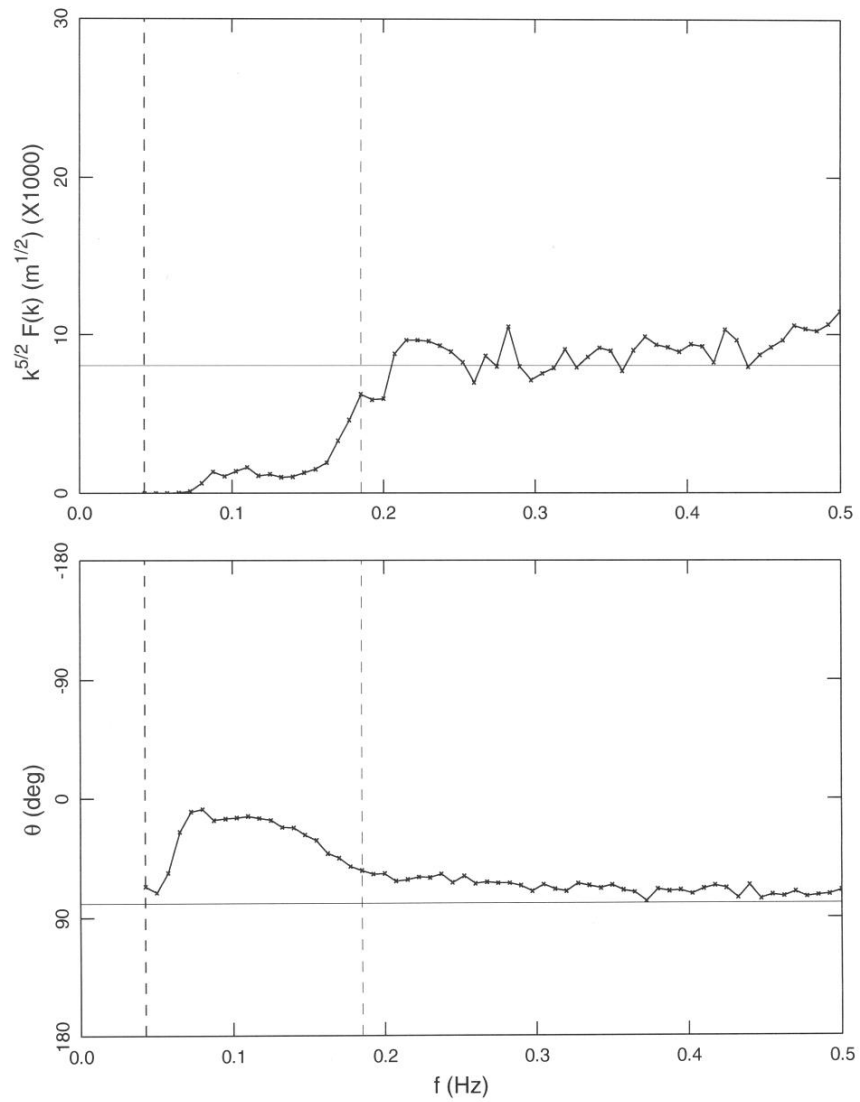


Figure 19. Upper panel shows compensated spectrum, lower panel mean direction as a function of frequency.

### FRF Waverider at 0210140700

	$H_{mo}$ (m)	$f_{p,ws}$ (Hz)	$\theta_p$ (deg)	$u_{10}$ (m/s)	$\theta_w$ (deg)	$h$ (m)
WR	2.56	0.1475	43	14.11	64	17.0

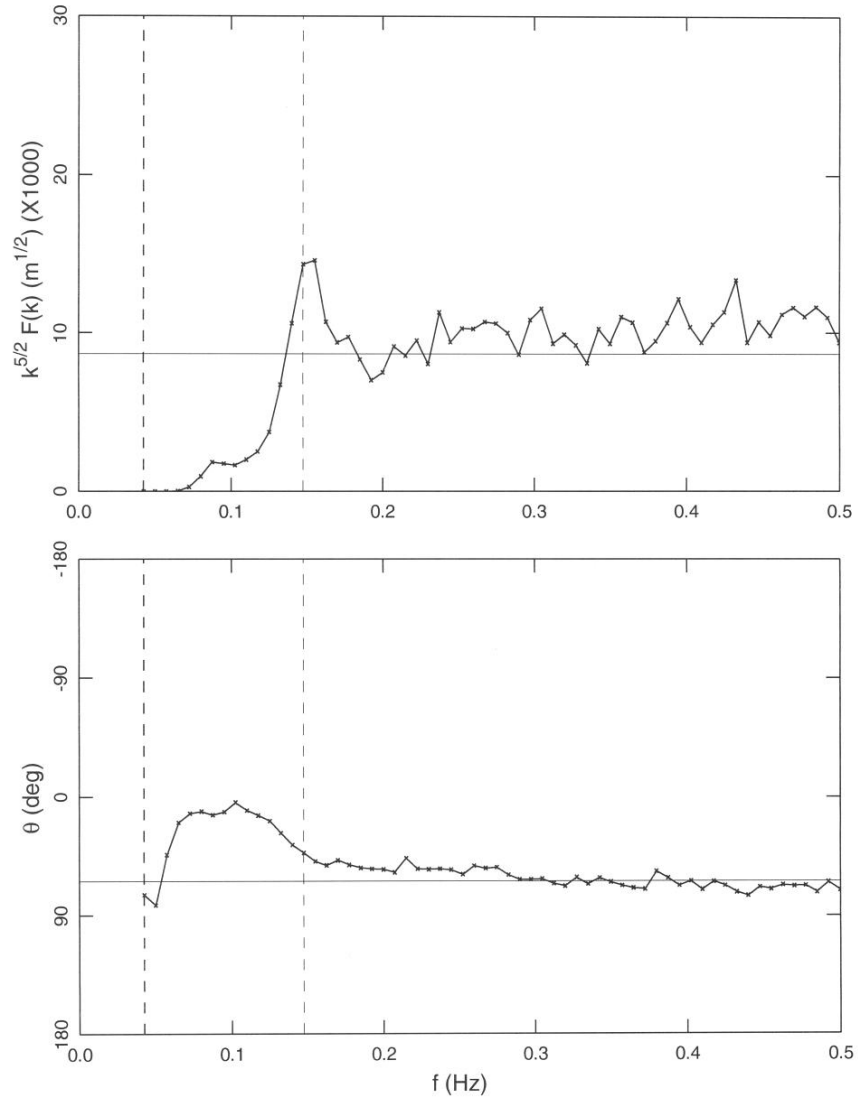


Figure 20. Upper panel shows compensated spectrum, lower panel mean direction as a function of frequency.

### FRF Waverider at 0210141900

	$H_{mo}$ (m)	$f_{p,ws}$ (Hz)	$\theta_p$ (deg)	$u_{10}$ (m/s)	$\theta_w$ (deg)	$h$ (m)
WR	2.14	0.1250	2	9.87	31	17.0

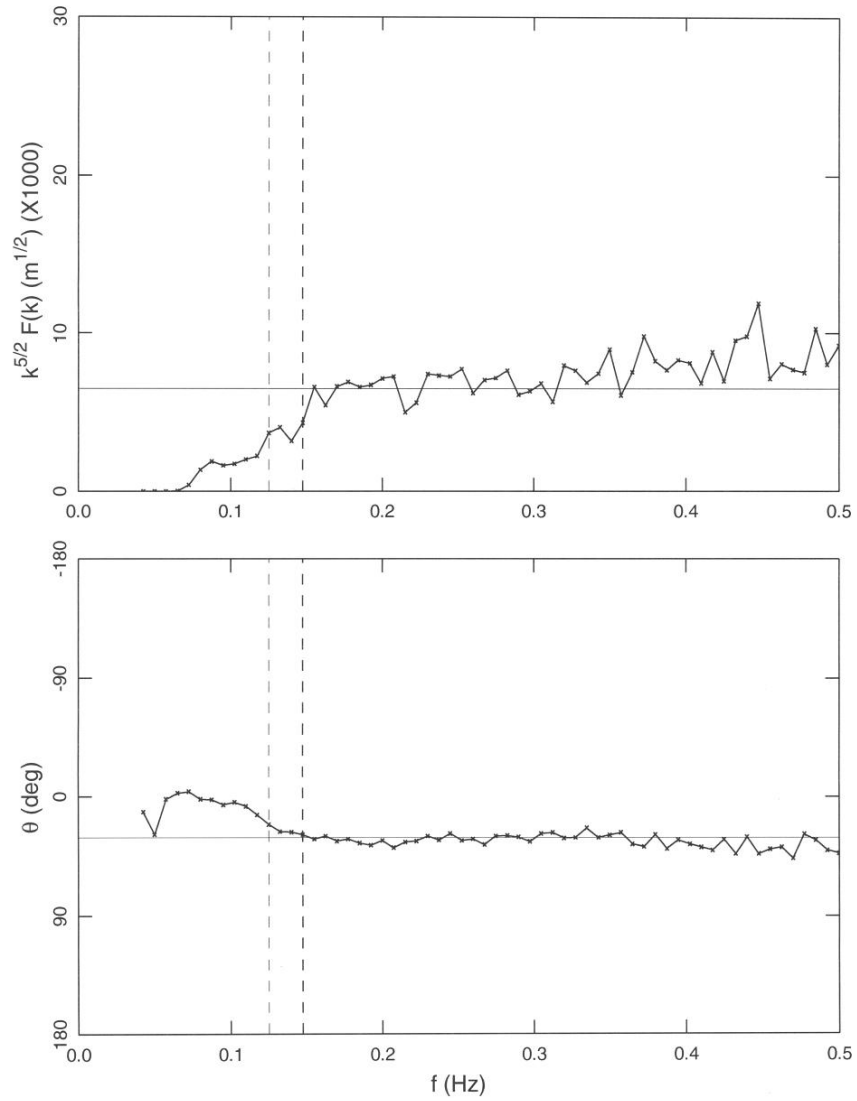


Figure 21. Upper panel shows compensated spectrum, lower panel mean direction as a function of frequency.

### FRF Waverider at 0210150100

	$H_{mo}$ (m)	$f_{p,ws}$ (Hz)	$\theta_p$ (deg)	$u_{10}$ (m/s)	$\theta_w$ (deg)	$h$ (m)
WR	1.97	0.1625	4	8.43	16	17.0

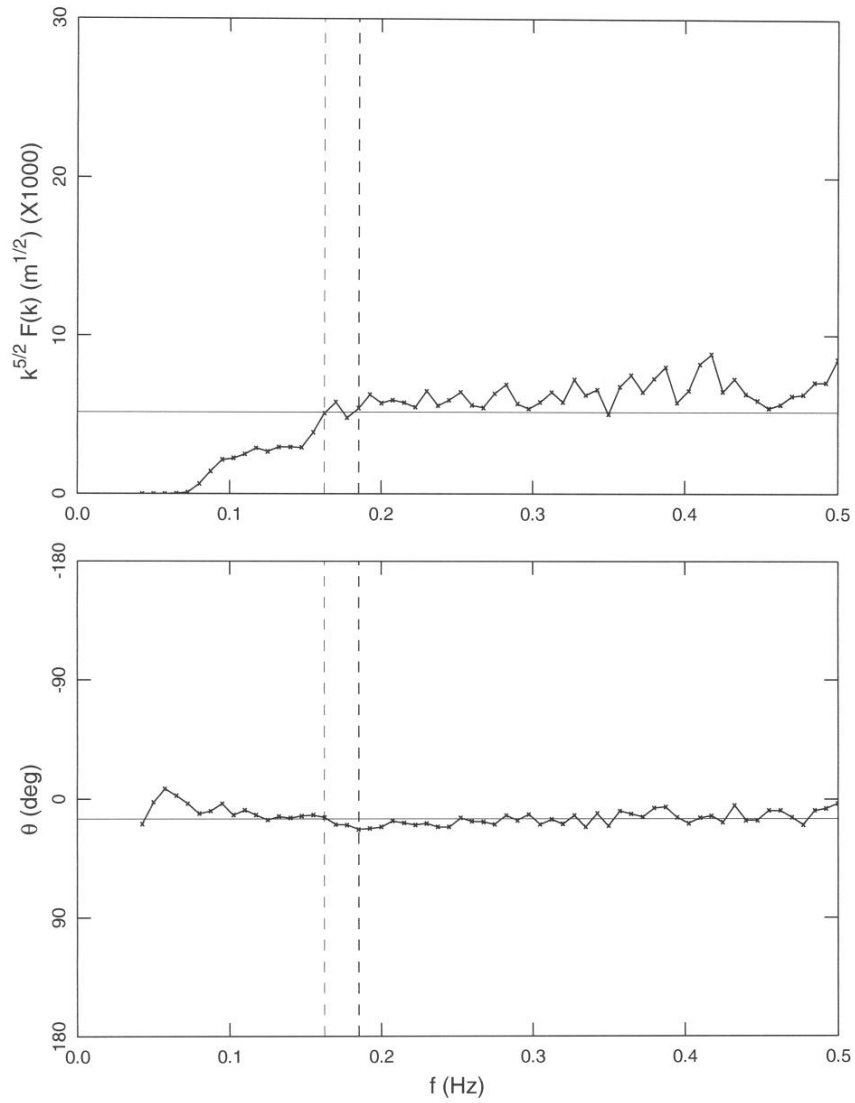


Figure 22. Upper panel shows compensated spectrum, lower panel mean direction as a function of frequency.

### FRF Waverider at 0210151300

	$H_{mo}$ (m)	$f_{p,ws}$ (Hz)	$\theta_p$ (deg)	$u_{10}$ (m/s)	$\theta_w$ (deg)	$h$ (m)
WR	2.41	0.1625	2	12.96	-3	17.0

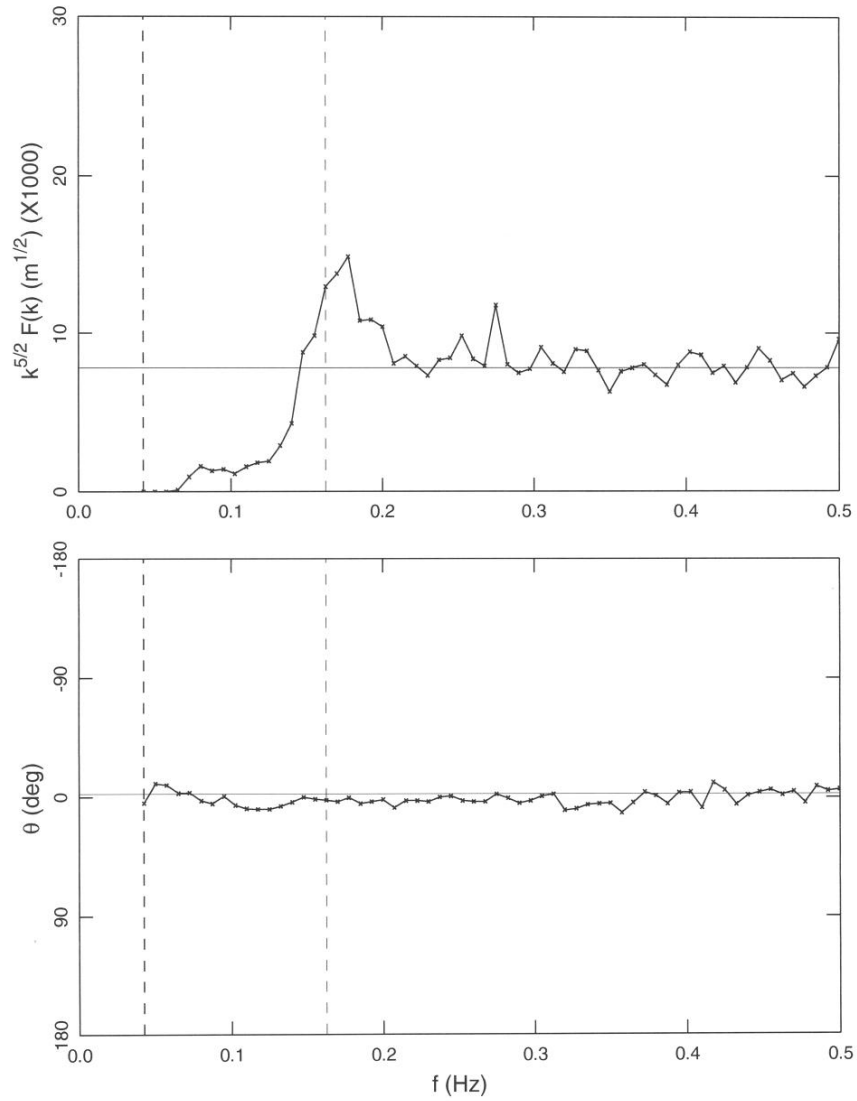


Figure 23. Upper panel shows compensated spectrum, lower panel mean direction as a function of frequency.

FRF Waverider at 0210151900

	$H_{mo}$ (m)	$f_{p,ws}$ (Hz)	$\theta_p$ (deg)	$u_{10}$ (m/s)	$\theta_w$ (deg)	$h$ (m)
WR	2.96	0.1400	2	15.78	-9	17.0

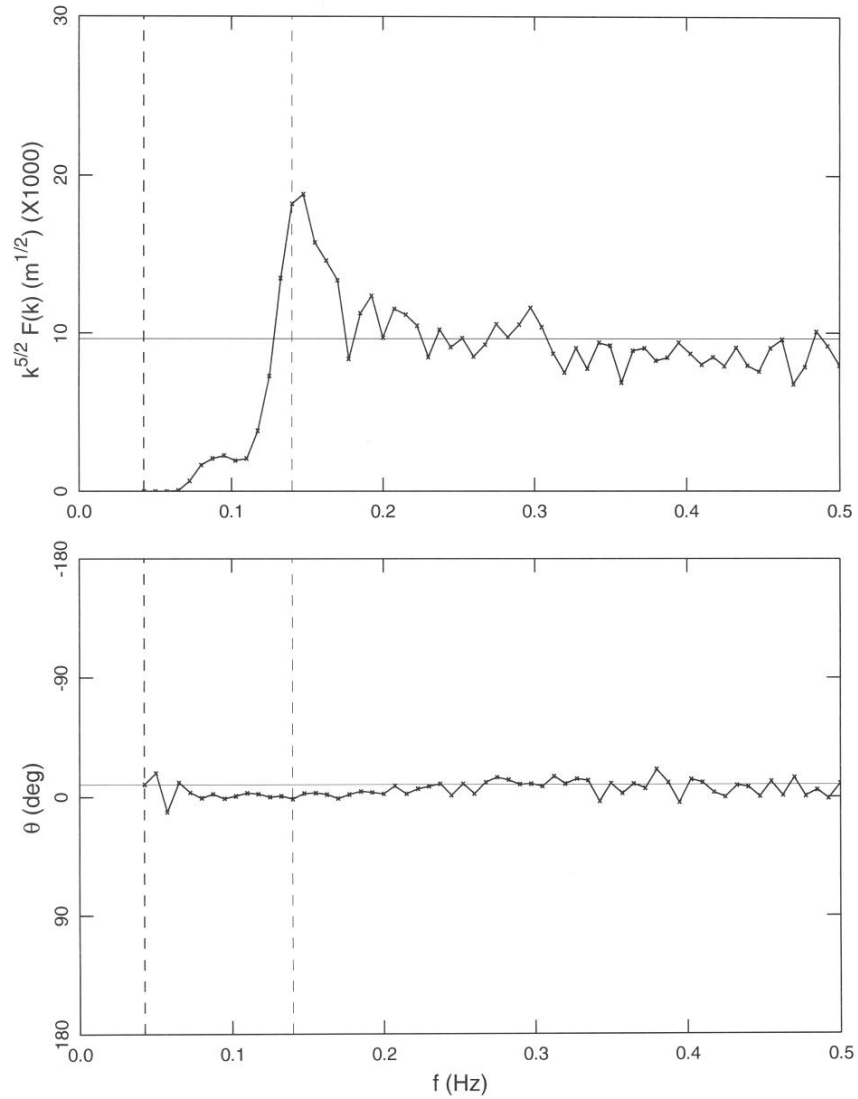


Figure 24. Upper panel shows compensated spectrum, lower panel mean direction as a function of frequency.

### FRF Waverider at 0210152200

	$H_{mo}$ (m)	$f_{p,ws}$ (Hz)	$\theta_p$ (deg)	$u_{10}$ (m/s)	$\theta_w$ (deg)	$h$ (m)
WR	3.55	0.1325	1	17.03	11	17.0

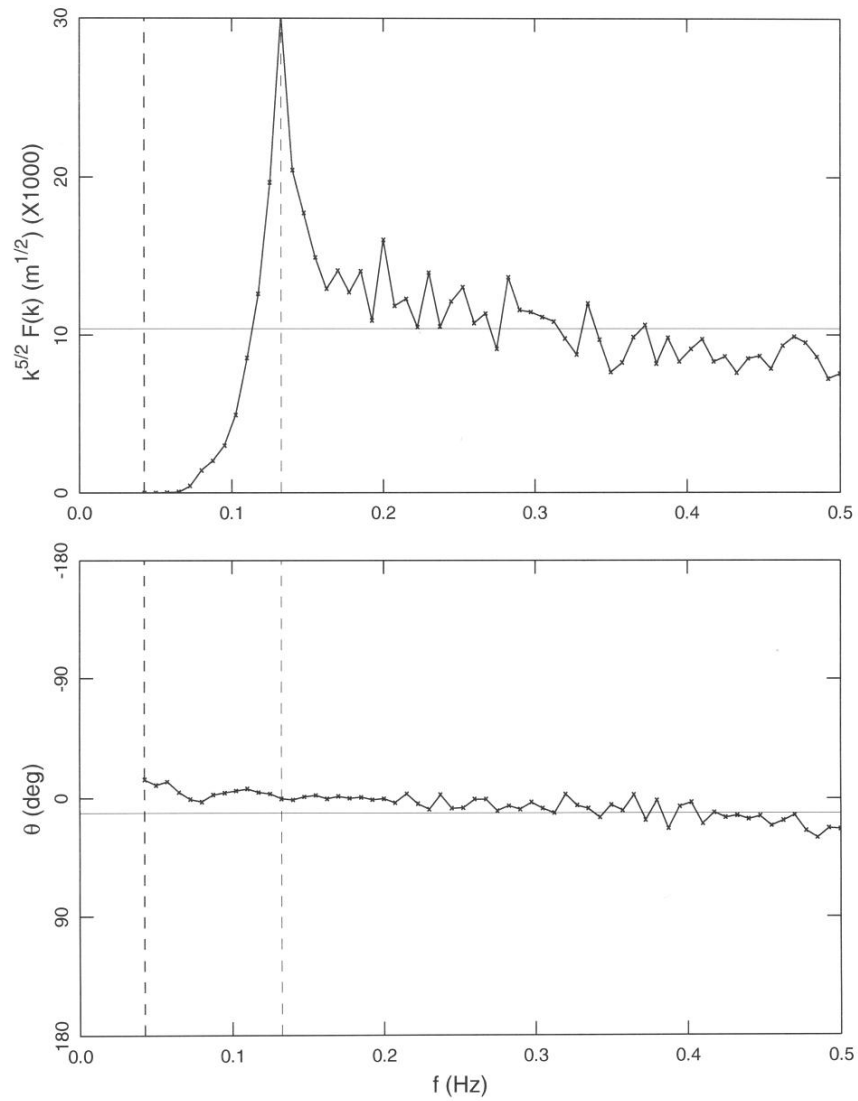


Figure 25. Upper panel shows compensated spectrum, lower panel mean direction as a function of frequency.

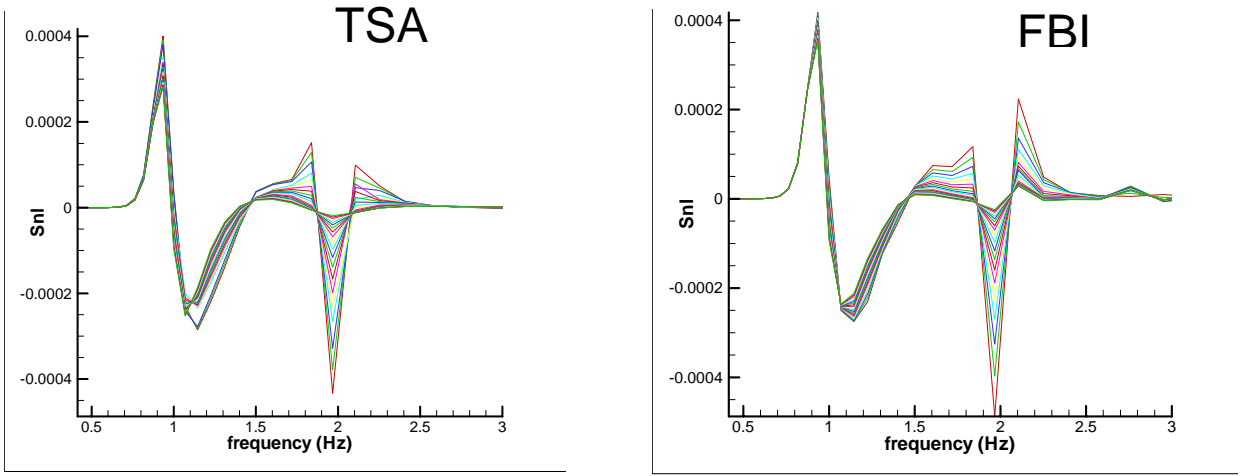


Figure 26. Comparison of nonlinear interactions due to a perturbation in TSA and FBI.

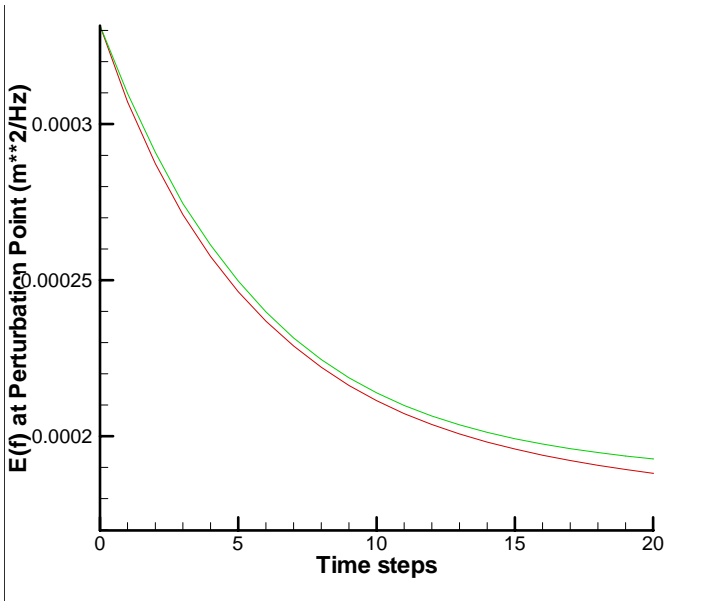


Figure 27. Comparison of decay of a perturbation in TSA (red) and FBI (green).